

# DESIGN STRATEGIES FOR REDUCING PERFORMANCE DEGRADATION DUE TO FROSTING OF DISPLAY CASE HEAT EXCHANGERS

**P. Verma**

Student, M&IE Department, University of  
Illinois at Urbana-Champaign, Illinois, USA

**C. W. Bullard**

Professor, M&IE Department, University of  
Illinois at Urbana-Champaign, Illinois, USA  
Tel.: +1-217-333-7734; fax: +1-217-333-1942  
e-mail: bullard@uiuc.edu

**P. S. Hrnjak**

Professor, M&IE Department, University of  
Illinois at Urbana-Champaign, Illinois, USA

## Abstract

Three design strategies for reducing defrost frequency and overall energy consumption of open supermarket display cases were evaluated: variable air flow operation; constant air flow operation; and fin staging. An experimentally validated simulation model for secondary refrigerant and constant operating conditions was extended (DX operation, ambient air infiltration, reduced air flow with frost buildup, and varying heat exchanger geometry) to simulate operation of open display cases, modelling the varying frost properties and operating conditions and their effect on heat exchanger performance. Results suggest that the defrost interval could be extended from 4.8 hours to 8 hours by employing a variable-speed fan to maintain constant air flow; the energy efficiency penalty was quantified in terms of increased fan and compressor energy requirements for comparison with energy savings resulting from less frequent defrosts. Fin staging is also shown to result in significant performance improvements, especially at low face velocities and high inlet humidities where most of the frosting occurs near the front of the heat exchanger.

## Nomenclature

A surface area,  $m^2$   
 af ambient air entrainment fraction  
 cfm air flow rate,  $cfm$   
 Dc tube outer diameter,  $m$   
 D<sub>h</sub> hydraulic diameter,  $m$   
 dP pressure drop,  $Pa$   
 f Darcy's friction factor  
 f<sub>th</sub> fin thickness,  $m$   
 Fs fin pitch,  $m$   
 h enthalpy of dry air,  $kJ/kg$   
 h<sub>a</sub> convective airside heat transfer coefficient,  $kW/m^2.K$   
 h<sub>ref</sub> refrigerant side heat transfer coefficient,  $kW/m^2.K$   
 j Colburn's dimensionless heat transfer coefficient  
 k<sub>fr</sub> thermal conductivity of frost,  $kW/m.K$   
 m<sub>fr</sub> total mass of frost deposited,  $kg$   
 m<sub>air</sub> air mass flow rate,  $kg/s$   
 m<sub>ref</sub> refrigerant mass flow rate,  $kg/s$   
 Q load on evaporator,  $kW$   
 p pressure,  $Pa$   
 r distance from the center of the tube,  $m$   
 Re Reynolds number  
 T temperature,  $^{\circ}C$   
 V<sub>max</sub> velocity of air based on free flow area,  $m/s$   
 w air absolute humidity,  $kg_{water}/kg_{air}$   
 x vapor mass fraction of refrigerant  
 y depth of each finite volume,  $m$

## Greek symbols

ρ density of air,  $kg/m^3$   
 ρ<sub>fr</sub> density of frost,  $kg/m^3$   
 δ<sub>fr</sub> frost thickness,  $m$

## Subscripts

a air  
 amb evaluated at store ambient air temperature  
 c tube outer surface,  $m$   
 case sum of radiation, lights and fan motor  
 dis evaluated at case discharge air temperature  
 dry dry  
 f fin  
 fr frost surface  
 o overall (fin and tube)  
 out outlet  
 r refrigerant  
 ret evaluated at case return air temperature  
 si base of the fin  
 so frost surface (fin and tube)  
 tb tube

## Introduction

Frost accumulation is a direct result of the heat and mass transfer from the moist air passing over the cold heat exchanger surfaces. Whenever the temperature of the evaporator surface is below the dew point temperature, moisture in the air condenses. If the surface temperature is below freezing, frost begins to form.

Supermarkets accounts for ~4% of the US electricity consumption with frozen and fresh food display cases representing most of the supermarket refrigeration load. Therefore it is essential to identify the ways in which frost buildup affects the efficiency of display cases. Then by exploiting the trade-offs among the underlying physical parameters, it is possible to reduce the impact of frost on the system performance.

Three frost related factors affect the rate of decrease in refrigerant evaporating temperatures (hence system efficiency): air flow blockage; change in air-side heat transfer coefficient; and the insulation effect of frost. Of these the reduction of air flow rate is most important because it degrades the air curtain, which separates the store ambient air from the refrigerated product. Deposition of frost on the evaporator coils increases the air-side pressure drop across the evaporator, ultimately decreasing the air flow rate and increasing the entrainment of warm and humid store air. Apart from air curtain degradation, the frost deposited on the surface of the evaporator has very low thermal conductivity and insulates the cold surface from the warmer air. However, as more frost is deposited over time, its density and thermal conductivity increases, thus reducing its insulation effect.

Various researchers (Padki et. al. 1989, Rite and Crawford, 1990, Davis et. al. 1998) have found that frost deposition is initially favorable as it reduces fin-tube contact resistance and rough frosted surface acts as fins, thus temporarily increasing air-side heat transfer coefficient. However, as the frost thickens the insulating effect becomes dominant and the heat transfer rate is reduced. Also due to frost accumulation, the free flow area is reduced, thereby increasing the velocity of air and hence its heat transfer coefficient. O'Neal and Tree (1985) have reviewed studies of frost formation in geometries such as flat plates, parallel plates, tubular, cylinders, annuli etc. and Kondepudi and O'Neal (1987) reviewed the effects of frost growth on extended surface heat exchanger performance.

In the past, heat pumps and air coolers have been the focus of various researchers to study frost growth and its effects. Oskarsson et al. (1990) presented heat pump evaporator models for operation with dry, wet and frosted surfaces. Senshu et al. (1990) and Kondepudi and O'Neal (1990) also considered the performance of heat pumps under frosting conditions. Sanders (1974) studied the frosting of air coolers.

However, little effort has been to model the effects of frost growth on supermarket display case heat exchanger performance and devise strategies to minimize such degradation. This paper focuses on evaluating three design strategies: variable air flow operation; constant air flow operation; and fin staging to reduce defrost frequency and overall energy consumption of supermarket display cases. In order to explore the aforesaid design strategies an experimentally validated simulation model (Verma et al. 2002) for secondary refrigerant and constant operating conditions was extended to simulate operation of open display cases, modelling the varying frost properties and operating conditions and their effect on heat exchangers. Identifying such design and operating conditions as fin staging, tube diameter, fin pitch and air flow rate, and exploiting tradeoffs among the aforesaid frost-related factors, it is possible to reduce the overall impact of frost deposition on system efficiency.

## Simulation of Display Case Evaporators

In order to study the effects of various parameters like air flow, inlet relative humidity, refrigerant inlet temperature, air inlet temperature on frost deposition and distribution, a heat exchanger frosting model was developed and validated (Verma et al. 2002) for a round tube, plain fin heat exchanger placed in a wind tunnel. A single-phase (secondary) refrigerant, methoxy-nonafluorobutane (HFE), was used to enable the refrigerant temperature glide to be controlled, and to enable real-time measurements of frost mass (plus evaporator) by suspending the heat exchanger in an open wind tunnel. The model was validated by comparisons to the experimental observations of Carlson et al. (2001) for air and refrigerant outlet temperatures, pressure drop across evaporator, frost mass and thickness and heat exchanger capacity, and generally good agreement was obtained for all.

To facilitate validation, the model developed by Wu et al. (2001) was used for indirect refrigeration and focused on air-side phenomena under constant running conditions i.e. steady inlet air and refrigerant temperatures and constant inlet relative humidity. Open supermarket display cases commonly employ DX (direct expansion) evaporators and experience variable running conditions owing to increasing infiltration through the air curtain. Hence in order to gain an in depth insight into the mechanisms by which the frost degrades evaporator performance and develop strategies to minimize such degradation, the quasi-steady finite volume heat exchanger model developed and validated for secondary refrigerant was extended to include the following: (1) DX operation (e.g.

refrigerant pressure drop, heat transfer coefficient, and superheat); (2) increasing entrainment of store air (as a function of air flow rate) and mixing with display case air, as frost blockage reduces air flowrate; (3) fan curve to simulate variable air flow response to frost buildup on the heat exchanger; and (4) staggered fin spacing and different package dimensions and coil geometry.

The overall approach was to begin by modeling a dry-surface DX evaporator, and then account for the deposition of frost, calculating its thickness distribution throughout the heat exchanger. At subsequent time steps, the frost thickness is added to the fin thickness.

### 1. Air Curtain Effects

Based on experimental data obtained from display case manufacturers, the variation of the air entrainment fraction ( $af$ ) could be expressed as a function of air flow rate (shown later). This infiltration load combined with other case loads such as lights, radiation, and 4 fans (each ~9W) was used to calculate the evaporator air inlet (return air) state.

$$(1-af) \cdot \dot{m}_{air} \cdot h_{dis} + af \cdot \dot{m}_{air} \cdot h_{amb} + Q_{case} = \dot{m}_{air} \cdot h_{ret} \quad (1)$$

$$(1-af) \cdot w_{dis} + af \cdot w_{amb} = w_{ret} \quad (2)$$

### 2. Heat Exchanger Geometry

A cross-counter flow heat exchanger geometry was considered which was divided into a certain number of finite volumes (equal to the number of tube rows in the air flow direction), as shown in Figure 1. At the first time step for each finite volume, a negligible amount of frost (0.2 mm thick) was assumed to exist on the heat exchanger surfaces. The tube diameter and fin thickness were updated as shown in upper left part of Figure 2. This assumption was to bypass the complex initial period of early (dendrite) frost growth and utilize equations that apply to the mature frost growth period. However, the magnitude chosen had no influence on any parameter after the first time step, as more and more frost was accumulated. At each time step the input parameters were obtained from previous time step (constant refrigerant inlet temperature, air flow from fan curve, mixed air inlet temperature and relative humidity from entrainment fraction).

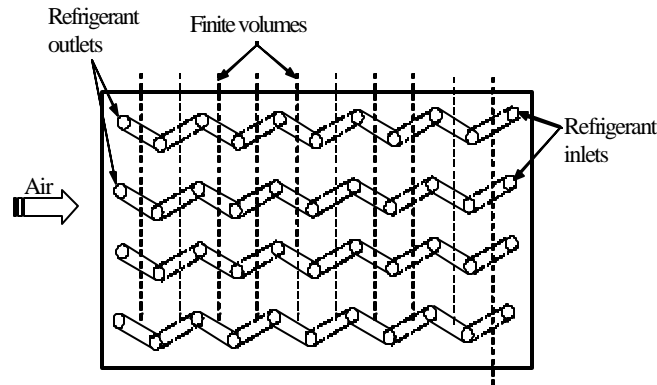


Figure 1. Heat exchanger Schematic

### 3. Heat Transfer and Pressure Drop Correlations

On the refrigerant side, the Gnielinsky (1976) correlation was used for single phase heat transfer, while the Wattleet and Chato (1994) correlation was used for two phase flow. The Souza and Pimenta (1995) correlation was used to determine the refrigerant side pressure drop.

The model was developed with the intention to explore a wide range of heat exchanger geometries, and  $j$  and  $f$ -factor correlations of Wang et al. (2000) were based on the largest and most diverse sets of data. Non-dimensionally the parameters describing typical display case evaporators lay barely within the parameter space of the correlation. However in absolute terms, both tube diameter and fin spacing lay outside the range of the correlation. The pitfalls become obvious when examining the friction factor correlation which increased monotonically with fin pitch for typical tubes dimensions (11 mm OD) and fin pitch ~8.5 mm. This absurd result led to us to replace the  $f$ -factor correlation with a straightforward superposition approximation of tube-plus-fin pressure drop given by Eq. 3 & 4, for each finite volume. The total air-side pressure drop determined matched closely with the experimental data

provided by Hussmann Corporation for a similar medium temperature display case coil. The Wang's j-factor correlation produced good agreement with the heat transfer data, so it was retained. For each finite volume, the average j-factor was determined by applying the Wang's correlation for the entire number of tube rows.

$$dP_f = f_f \cdot \frac{y}{D_h} \cdot \frac{r \cdot V_{\max}^2}{2} \quad (3)$$

$$dP_{tb} = f_{tb} \cdot \frac{r \cdot V_{\max}^2}{2} \quad (4)$$

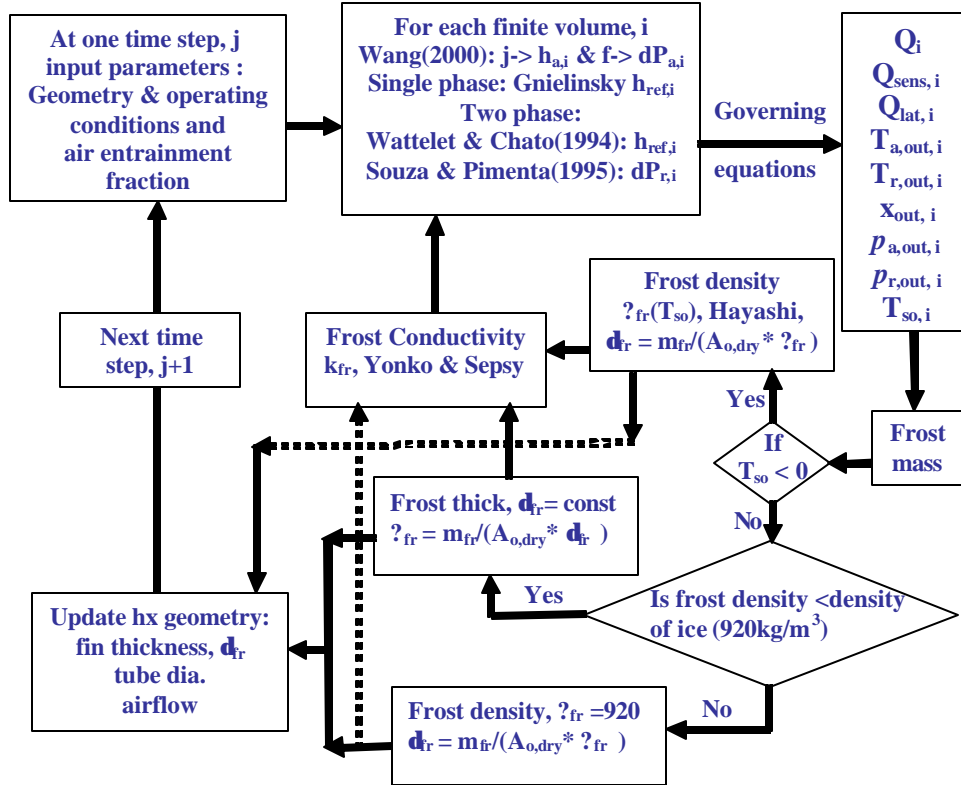


Figure 2 Structure of the model

Where,  $D_h$  is the hydraulic diameter based on the free flow passage assuming channel flow between two fins, and  $f_f$  and  $f_{tb}$  are determined using Churchill's (1977) f-factor correlation and Zhukauskas' correlation for staggered tube bundle arrangement given in Incropera and DeWitt (1996) respectively.

#### 4. Heat and Mass Transfer

The frosting rate and sensible, latent and total heat transfer was computed in the same manner (using the heat and mass transfer analogy, air and refrigerant heat transfer and rate equations) as Verma et al. (2002). Figure 3 shows part of a finite volume with fin and tube surface covered with frost. The heat exchanger was divided into enough finite volumes to warrant using the arithmetic mean temperature of air and refrigerant for one-dimensional computation of heat transfer for each finite element.

#### 5. Frost Accumulation Process

The next step, as indicated in Figure 2, was to calculate the frost thickness (from frost mass deposited and frost density) at this time step, and use it to update the fin thickness and tube outer diameter and for the next time step.

For a finite volume where the frost surface temperature was below the freezing point at all time steps, Hayashi's (1977) correlation given by the following equation was used.

$$r_{fr} = 650 e^{0.277 T_{so}} \quad (5)$$

That correlation however, has a limited range, so a different approach must be taken as the frost surface temperatures approach 0°C. At any time step, when the equilibrium equations predicted a frost surface temperature greater than or equal to 0°C, it was assumed that liquid condensate would permeate the frost layer and freeze increasing its density until the density of frost reached that of ice at the freezing point (920 kg/m<sup>3</sup>), while the frost thickness remains constant.

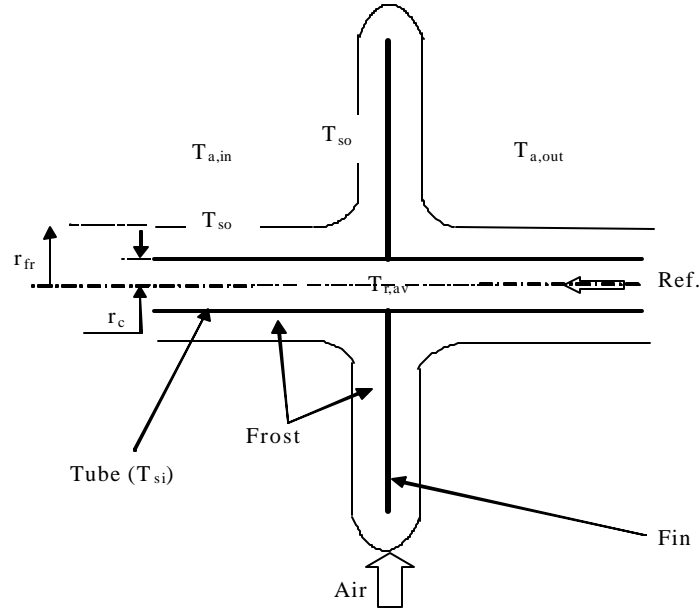


Figure 3. Heat transfer from the air through the frost layer, tube and fin to the refrigerant

The Yonko and Sepsy (1967) correlation (Eq. 6) was used to determine the frost conductivity as a function of frost density. Yonko and Sepsy measured frost thermal conductivity over a wide range of frost surface temperatures (-30°C to -5.7°C), and their correlation is limited to  $\rho_{fr} < 576 \text{ kg/m}^3$ . However their correlation when extrapolated to the density of ice predicts the thermal conductivity of ice within 10% of the actual value, so extrapolation was allowed in the simulations.

Finally using the determined frost thickness, the tube diameter and fin thickness were updated for each finite volume. Also the reduced airflow rate resulting from the increase in the air-side pressure drop was determined from the fan curve and subsequently used in the next time step.

With known current values for the frost thermal conductivity and frost thickness, the frost surface temperature and the additional mass deposition was computed simultaneously by solving the governing equations for the next time step.

$$k_{fr} = (0.02422 + 7.214 \cdot 10^{-4} \cdot r_{fr} + 1.1797 \cdot 10^{-6} \cdot r_{fr}^2) / 1000 \quad (6)$$

If at some future time step, the computed frost surface temperature drops below 0°C for e.g. due to the effect of air flow blockage, the aggregate frost density was assumed to remain constant for that time step, while the thickness was increased due to additional mass deposition. When calculations proceeded to the next time step, the simulation reverted to calculating frost density and thickness as described above, depending on whether mass transfer occurred as liquid or frost deposition.

If the frost density reached the density of ice (920 kg/m<sup>3</sup>), and liquid condensation continued, it was assumed that the incremental frost deposition occurred at the density of ice, 920 kg/m<sup>3</sup> and the frost thickness increased accordingly. Once the frost surface temperature reached 0°C, further decrease or increase would depend upon whether the effect of increased frost thermal conductivity (reduced insulation effect) outpaced the effect of increased return air temperature (due to increased air entrainment) or vice versa. If at any time step, the simulations resulted in the base temperature of the fin ( $T_{si}$ ) to be above 0°C, the above assumptions of liquid condensate seeping into the frost layer would not hold true and melting would occur. Equations to simulate melting were not included in the model, so the outputs were monitored to ensure that the simulations remained within their applicability.

All of the above adjustments for frost surface temperatures approaching 0°C occurred at the leading edge of the heat exchanger (only first finite volume) where the warmest air (at return air temperature ~4.5°C) came into contact with the superheated refrigerant tubes. Subsequent finite volumes had lower inlet air temperatures and also the

saturation temperature of the refrigerant was below freezing (only a fraction of the first finite volume superheated). Being limited to the leading edge, these assumptions did not have a significant impact on the heat exchanger geometry because the frost thickness in the superheated zone of the heat exchanger (leading edge) was the least (as shown below) and so had insignificant effect on the air curtain degradation.

## Evaluation of Design Strategies

To illustrate the capabilities of the simulation model, several strategies for decreasing defrost frequency were explored. Recall that frost deposition on the evaporator surface reduces the air flow rate due to an increase in the air-side pressure drop, insulates the air from the evaporator surface and alters the air-side heat transfer coefficient. There is significant potential to minimize adverse impacts through optimal selection of design parameters (e.g. fin spacing, fin thickness, tube diameter, package dimensions) and operating variables (e.g. air flow rate, evaporating temperature, refrigerant mass flow rate, return air temperature and humidity).

For open display cases where air curtain integrity defines the criterion for defrost initiation, most design and operating parameters are fixed due to geometrical constraints and/or case ambient (store air) conditions. The following analysis assumes that the overall package dimensions of the evaporator are fixed due to the size of the display case, and the return air temperature and humidity are determined by the entrainment of the store air.

### 1. Variable Air Flow (Baseline Operation)

To understand the mechanisms by which frost degrades evaporator performance, an 11 row (44 passes in 4 refrigerant circuits) 8' medium-temperature open display case evaporator (2°C superheat) equipped with four fans running in parallel (combined fan curve given by Eq. 7) was considered. Simulations quantified the air-side pressure drop, hence the reduction of air flow rate via the fan curve, on evaporator capacity and defrost interval. The air entrainment fraction (expressed as a function of air flow rate) given by Eq. 8 was determined from the manufacturer data for variations over time of return and discharge air temperatures.

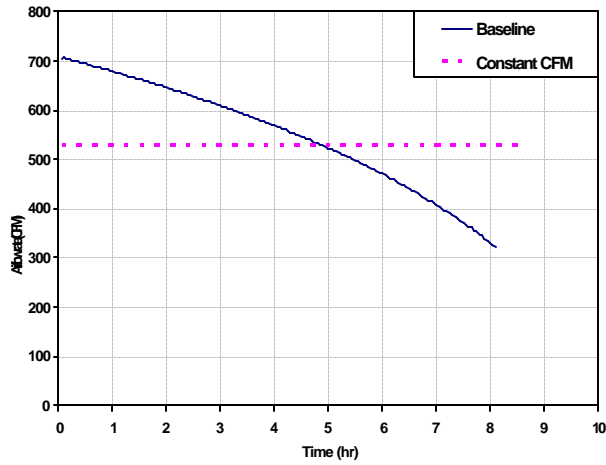
$$dP_{fan} = -9.98 \cdot \dot{V}_{air}^2 - 115 \cdot \dot{V}_{air} + 81.14. \quad (7)$$

$$af = 0.783 - 1.66 * 10^{-3} cfm + 1.16 * 10^{-6} cfm^2 \quad (8)$$

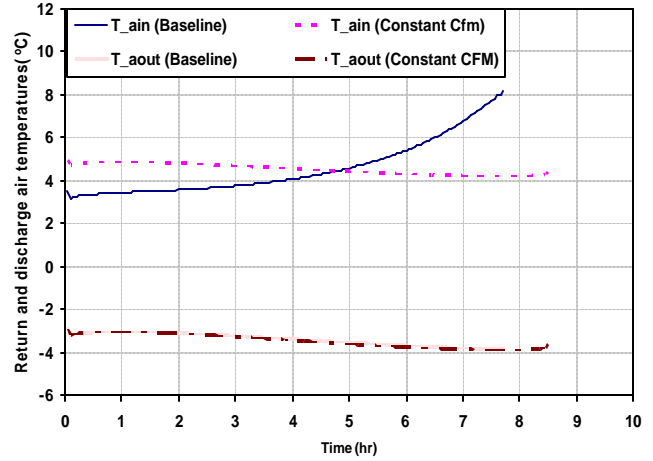
For the display case simulated the air curtain breaks down and defrost is initiated at ~530 cfm, at a sensible capacity of ~2.6 kW corresponding to -3.3°C discharge air temperature. To achieve an acceptable defrost interval, the case was designed to deliver (at startup following defrost) 33% more air flow rate (~707 cfm) corresponding to a sensible capacity of ~2.8 kW, with the same discharge air temperature as seen in Figures 4(a)-(d). Defrost was then timed to occur after ~4.8 hours of operation to allow air flow to remain always above the breakdown during the entire cycle. The simulations were continued past the defrost time, until the algorithm failed after ~8 hours of running when frost had occluded 77% of the initial free flow area.

The air entrainment fraction increases as air flow rate decreases, causing higher return air temperatures as shown in Figure 4(b). The discharge air temperature decreases slightly as a result of two offsetting trends: decreasing air flow; and increasing return air temperature. The reduction in free flow area due to the blockage effect of the frost actually increases the air-side heat transfer coefficient (velocity increases faster due to area constriction than it decreases due to air-side pressure drop).

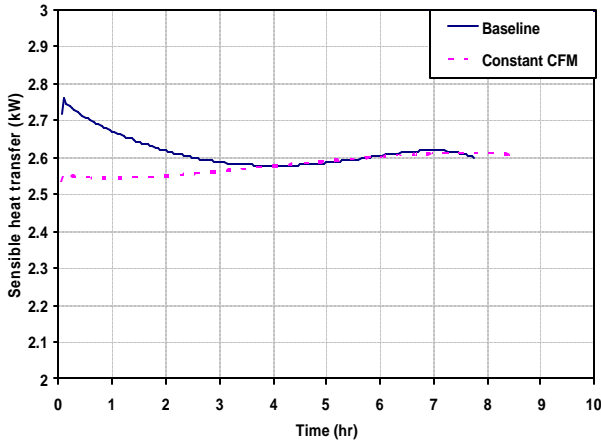
Prior to defrost initiation, sensible capacity declined because the decreasing air flow rate dominated the increasing return air temperature, as shown in Figure 4(c). If defrost was not initiated at 4.8 hours, the simulations showed that changes in the return air temperature would become dominant, causing the sensible capacity to rise.



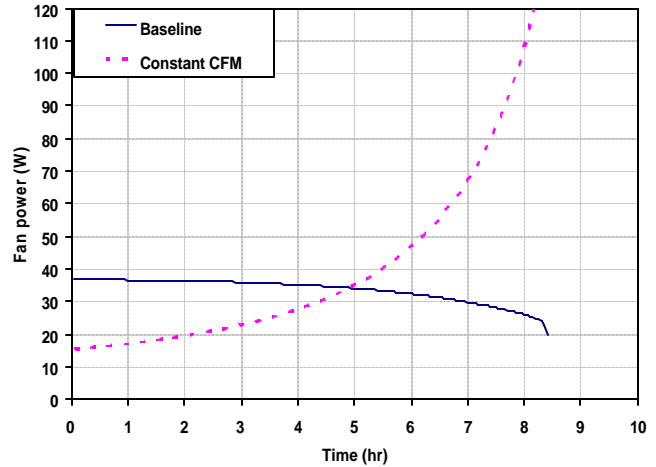
(a) Air flow rate



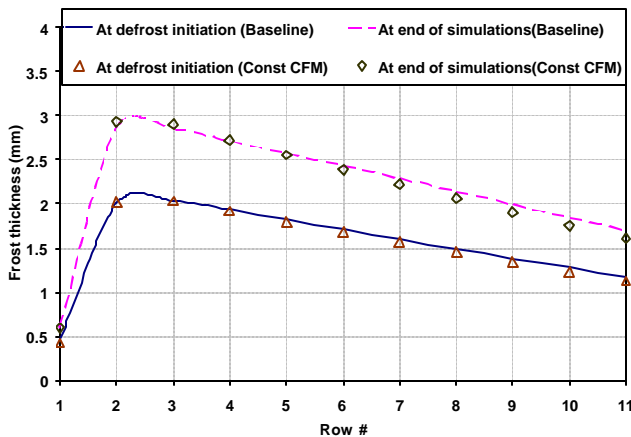
(b) Return and discharge air temperatures



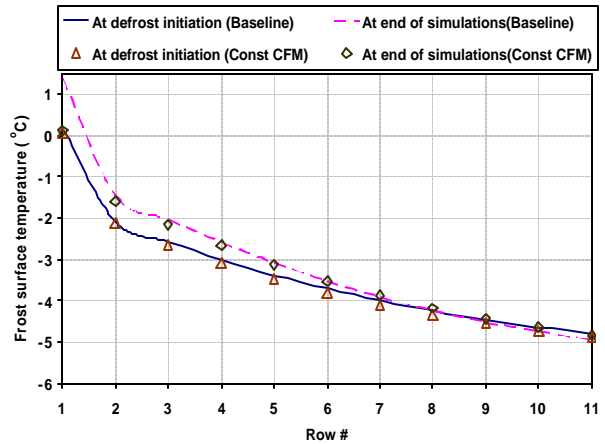
(c) Sensible capacity



(d) Fan power



(e) Frost thickness distribution



(f) Frost surface temperature distribution

Figure 4. Comparison of variable (baseline) and constant air flow operation

## 2. Constant air flow

Time between defrosts could theoretically be extended by using a variable-speed fan, and gradually increasing its voltage to maintain a constant 530 cfm as frost blocked the free flow area. The results are designated “constant cfm” in Figures 4(a)-(f). Since the “constant air flow” is initially lower, air curtain entrainment is ~23%, compared to ~19% in the baseline; presumably this could be improved by redesigning the curtain for constant air flow, but that option was not considered in this example. Figure 4(b) shows that the return air temperature was initially higher for constant air flow and declines steadily. However, it increased sharply after ~5 hours for baseline operation as air flow rate dropped below the breakdown level as frost blockage continued to reduce air flow rate and increase entrainment in the standard display case.

For constant air flow operation (with variable-speed fan) a lower refrigerant temperature was selected (-6.3°C, compared to -6.2°C for the baseline operation) to ensure that the initial discharge air temperature was the same as for baseline operation. This produced a sensible capacity (equal to the breakdown value, 2.6 kW) lower than the baseline design capacity (2.8 kW). Figure 4(c) also shows how the sensible capacity for constant air flow operation increased slowly but steadily over time as the air-side heat transfer coefficient increased due to blockage of the free flow area. With sensible capacity increasing and return air temperatures dropping with time, the discharge air temperature dropped over time (identically as the baseline operation) as shown in Figure 4(b).

Unexpectedly, for constant air flow operation, the frost thickness and deposition rates were almost the same as baseline operation (Figure 4(e)), because the surface temperature distribution was the same for both (Figure 4(f)). The simulations revealed that the return air humidity was higher (due to higher store air entrainment) for the constant air flow operation, but this higher absolute humidity gradient between the air and frost surface was offset by the lower air-side heat (mass) transfer coefficient associated with the lower (constant) air flow rate.

As seen in Figure 4(d), the fan power requirement for the baseline operation was initially higher and dropped monotonically over time as air flow rate decreased due to frost blockage. To maintain constant air flow operation, with air-side pressure drop increasing over time, the fan power requirement increased from ~15W (initially) to ~100W (after 8 hours) to maintain a constant air flow. Averaged over 8 hours, the fan power was 28% (~7 W) greater than the 4.8 hour average for the baseline (constant speed fan) operation.

## 3. Fin Staging

Another strategy explored for decreasing defrosting frequency was fin staging. By varying fin pitch along the air flow direction variations in frost thickness can be accommodated. Several patterns chosen based on manufacturing feasibility (e.g. multiples of 2 and not in fractions as shown in Figure 5) are listed in Table 1 along with the respective refrigerant inlet temperature. The patterns were chosen so that the total air-side pressure drop was the same as for the baseline operation and so the total amount of fin surface area as well as its distribution varied from pattern to pattern. The designation “1-4/5-11” in Table 1 denotes a type of fin staging where rows 1-4 contain half as many fins as rows 5-11. For all simulations, the total number of fins and their distribution was chosen to have the same initial air flow rate (i.e. same overall air-side pressure drop) as the baseline operation. Also the refrigerant inlet temperature was chosen to give the same display case discharge air temperature as in baseline operation. Holding initial air flow rate and case discharge air temperature constant would ensure that the product temperature at the start of each simulation was the same as that for the baseline. The change in COP was estimated using a performance map for an R404A scroll refrigeration compressor (Copeland ZS45K4E scroll) typically used in supermarket applications.

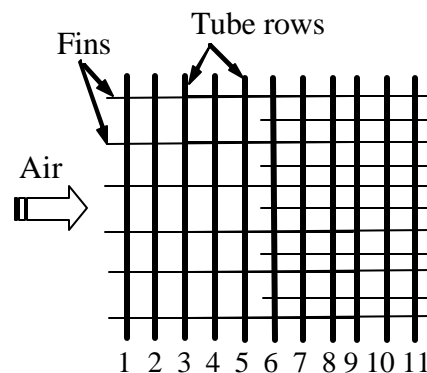
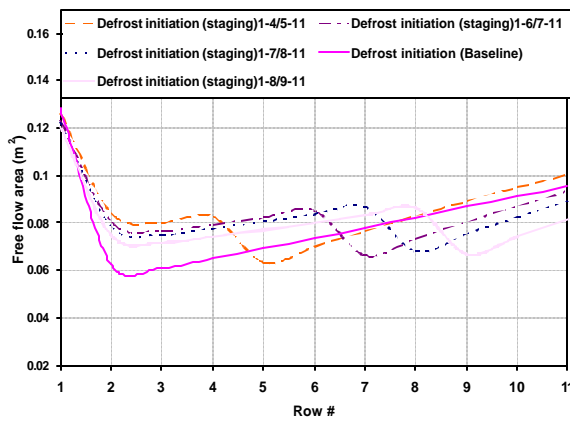


Figure 5 Fin staging schematic

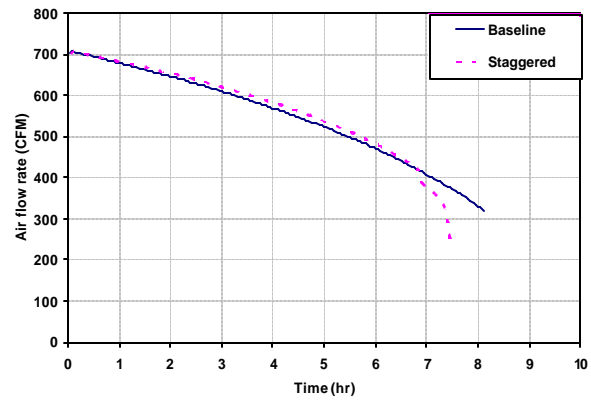
Figure 6(a) compares baseline and various fin staging simulations, in terms of free flow area at each tube row along air flow direction. It was found that the most uniform free flow area distribution was obtained when the transition to twice fin density occurred at 9<sup>th</sup> tube row. However, not much runtime was gained in terms of the defrost initiation time, (i.e. time at which air flow has decreased by 33%) due to loss of fin surface area. The maximum time gained (~15 minutes) was for fin staging designated “1-4/5-11” in Table 1 and the comparison between the baseline operation and this particular fin staging is shown in Figures 6(b) & (c).

Table 1 Comparison of evaporating temperature, % change in COP and total air-side surface area for uniform fin pitch (baseline) and fin staging simulations

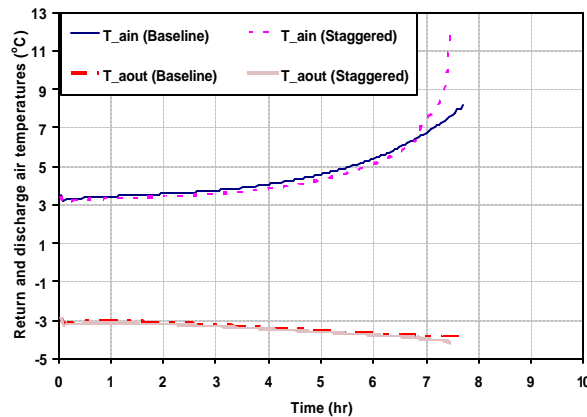
Designation	Fs (mm)	T <sub>r,in</sub> (°C)	COP (%)	A <sub>o</sub> (%)
Baseline	Row # 1-11 (8.3)	-6.2	0.00	0.0
1-4/5-11	Row # 1-4 (12.97) Row # 5-11 (6.36)	-5.6	+1.42	5.2
1-6/7-11	Row # 1-6 (12.24) Row # 7-11 (6.00)	-5.8	+0.94	-0.3
1-7/8-11	Row # 1-7 (11.94) Row # 8-11 (5.85)	-5.9	+0.71	-3.8
1-8/9-11	Row # 1-8 (11.72) Row # 9-11 (5.74)	-6.2	0.00	-8.0



(a) Free flow area across hx



(b) Air flow rate



(c) Case return and discharge air temperatures

Figure 6 Comparison of uniform fin pitch (baseline) and fin staging simulations

However, by moving the transition tube row in the upwind direction, the refrigerant inlet temperature could be raised and COP improved. For example with “1-4/5-11” type of staging, the refrigerant inlet temperature could be raised from -6.2°C (baseline operation) to -5.6°C (up 10%), increasing COP by as much as 1.4%. The time variation of return and discharge air temperatures, capacity and total frost mass deposition was found to be the same for both baseline and staggered fin operations. Similar trends were observed for all fin staging simulations shown in Table 1.

## Conclusions

To understand the mechanisms by which frost degrades evaporator performance, a simulation model developed and validated for secondary refrigerant was extended to simulate varying operating conditions of supermarket display case direct expansion heat exchanger. Simulations were done to explore two strategies for reducing the defrost frequency of a medium temperature supermarket display case: constant air flow rate (variable speed fan); and fin staging.

The results shown in Figures 4(a)-(f) suggest that the defrost interval could be extended from ~4.8 to about 8 hours by using a variable-speed fan to maintain a constant air flow. A net energy savings would result only if the additional energy consumption due to increased fan (28%) and compressor power were offset by the energy savings resulting from less frequent defrosting. It is worth mentioning that the product temperature may be lower with less frequent defrosts due to reduced number of shock cycles a product goes through with each defrost cycle.

With the help of a particular example it was demonstrated how fin staging may provide significant performance enhancements, even when the baseline frost distribution is already quite uniform. In other situations where frost blocks the front rows very early (e.g. when face velocity is lower or inlet humidity is higher), the fin staging can extend defrost intervals even more, while at the same time reducing the cost of fin material required.

## Acknowledgement

This work was supported by the US Department of Energy, Office of Building Technology, State and Community Programs under contract DE-AC05-00OR22725 with UT-Battelle, LLC., and the 28 member companies of Air Conditioning and Refrigeration Center, University of Illinois at Urbana-Champaign.

## References

- Carlson, D. M., Hrnjak, P. S., and Bullard, C. W. 2001. Deposition, distribution, and effects of frost on a multi-row heat exchanger performance. ACRC TR-183, University of Illinois at Urbana-Champaign, IL.
- Churchill, S. W. 1977. Friction-factor equation spans all fluid-flow regimes. *Chemical Engineering*, pp 91-92.
- Davis M. A., Jacobi A. M., and Hrnjak P. S. 1996. Evaporator calorimeter: The study of overall heat transfer performance. ACRC TR-107, University of Illinois at Urbana-Champaign, IL.
- Gnielinski, V. 1976. New equations for heat and mass transfer in turbulent pipe and channel flow. *Chemical Engineering*, 16:359-368.
- Hayashi, Y., Aoki, K., and Yuhura, H. 1976. Study of frost formation based on a theoretical model of the frost layer. *Trans. Japan Society Mechanical Engineers*, 40:885-899.
- Hayashi, Y., Aoki, A., Adachi, S., and Hori, K. 1977. Study of frost properties correlation with frost formation types. *Journal of Heat transfer*, 99: 239-245.
- Incropera, F. P., and DeWitt, D. P. 1996. *Fundamentals of heat and mass transfer*. John Wiley & Sons, 4<sup>th</sup> Edition.
- Kondepudi, S. N., and O’Neal, D.L. 1987. The effect of frost growth on extended surface heat exchanger performance—a review. *ASHRAE Transactions*, 93(2):258-274.
- Kondepudi, S.N., and O’Neal, D. L. 1990. The effects of different fin configurations on the performance of finned-tube heat exchangers under frosting conditions. *ASHRAE Transactions*, 96(2).
- O’Neal, D. L., and Tree, D. R. 1985. A review of frost formation in simple geometries. *ASHRAE Transactions*, 91:267-281.

- Oskarsson, S. O., Krakow, K. I., and Lin, S. 1990. Evaporator models for operation with dry, wet and frosted finned surfaces, Pt. I and II. ASHRAE Transactions, 96(1): 373-392.
- Padki, M. M., Sherif S. A., and Nelson R. M. 1989. A simple method for modelling the frost formation phenomenon in different geometries. ASHRAE Transactions, 95(2): 1127-1137.
- Rite, R. W., and Crawford R. R. 1990. The effect of frosting on the performance of domestic refrigerator-freezer finned tube evaporator coils. ACRC TR-01, University of Illinois at Urbana-Champaign, IL
- Sanders C. Th. 1974. Frost formation: The influence of frost formation and defrosting on the performance of air coolers. Ph.D. Thesis. Technique Hogeschool, Delft, Netherlands.
- Senshu, T., Yasuday H., Oguni K., and Ishibane K. 1990. Heat pump performance under frosting conditions Part 1 and 2. ASHRAE Transactions 96(1):324-336
- Souza A. L., and Pimenta M. M. 1995. Prediction of pressure drop during horizontal two-phase flow of pure and mixed refrigerants. ASME Conf. Cavitation and multiphase flow, HTD 210:161-171.
- Wang, C. C., Chi K. Y., and Chang C. J. 2000. Heat transfer and friction characteristics of plain fin-and-tube heat exchangers, Part II: Correlation. Int. J. of Heat and Mass Transfer, 43(15): 2693-2700.
- Wattelet, J. P., and. Chato, J. C. 1994. Heat transfer flow regimes of refrigerants in a horizontal-tube evaporator. ACRC TR-55 University of Illinois at Urbana-Champaign.
- Wu, Y., Verma, P., Bullard, C. W., and Hrnjak, P. S. 2001. Simulating the performance of a heat exchanger during frosting. ACRC TR-186, University of Illinois at Urbana-Champaign, IL
- Yonko, J. D., and. Sepsy, C. F. 1967. An investigation of the thermal conductivity of frost while forming on a flat horizontal plate. ASHRAE Transactions 73(II): I.1.1-I.1.11.
- Verma P., Carlson, D. M., Wu, Y., Bullard, C. W., and Hrnjak, P. S. 2002. Experimentally validated model for frosting of plain-fin-round-tube heat exchanger. IIR proceedings of the conference, "New Technologies in Commercial Refrigeration".